JACS
JOURNAL OF THE AMERICAN CHEMICAL SOCIETY
pubs.acs.org/JACS
Communication

Multi-active Site Dynamics on a Molecular Cr/Co/Se Cluster Catalyst

Jonathan A. Kephart, Benjamin S. Mitchell, Werner Kaminsky, and Alexandra Velian*

Cite This: J. Am. Chem. Soc. 2022, 144, 9206–9211
Read Online
ACCESS | Metrics & More | Article Recommendations | Supporting Information

ABSTRACT: This study uncovers the interconnected reactivity of the three catalytically active sites of an atomically precise nanocluster $Cr_3(py)_3Co_6Se_8L_6$ (**1**$(py)_3$, L = Ph_2PNTol^-, Ph = phenyl, Tol = 4-tolyl). Catalytic and stoichiometric studies into tosyl azide activation and carbodiimide formation enabled the isolation and crystallographic characterization of key catalytically competent metal-imido intermediates, including the tris(imido) cluster **1**$(NTs)_3$, the catalytic resting state **1**$(NTs)_3(CN^tBu)_3$, and the site-differentiated mono(imido) cluster **1**$(NTs)(CN^tBu)_2$. In the stoichiometric regime, nitrene transfer proceeds via a stepwise mechanism, with the three active sites engaging sequentially to produce carbodiimide. Moreover, the chemical state of neighboring active sites was found to regulate the affinity for substrates of an individual Cr-imido edge site, as revealed by comparative structural analysis and CN^tBu binding studies.

Understanding and controlling catalytically active sites is the holy grail of nanoscale catalysis,[1−3] promising to unlock fundamental insights into their mechanism and facilitate the creation of catalysts designed for specific transformations. The concept of "active sites" in heterogeneous catalysis was first introduced by Taylor nearly a century ago,[4] but their identity as low-coordinate surface sites was not experimentally verified until decades later by Ertl.[5] To date, identifying active sites experimentally and elucidating their mechanism of action remains exceedingly difficult. Although surface characterization techniques can provide atomic level understanding of the identity, location, and even mechanism of active sites in well-defined surfaces,[5−8] they withhold critical details into bonding and electronic structure that are more easily accessed using the myriad strategies available to molecular chemists. Atomically precise nanoclusters could enable incorporating molecular precision in the design and mechanistic study of active sites (Figure 1).[2,3] Relative to their bulk counterparts, these platforms exhibit large surface-to-core ratios, which maximize the number of possible active sites, and their catalytic selectivity and performance can be systematically tuned by altering size,[6,9] morphology,[10] or composition.[7,11−13] However, in order to unlock their potential for catalysis, synthetic innovations are required to prepare monodisperse clusters at scale and to exercise precise control over their surface chemistry and composition.

A large library of molecular ligand-stabilized transition metal nanoclusters exists, which are solution processable and have discrete chemical compositions.[14−16] Although the vast majority are not catalytically competent, some shed light on the physicochemical processes that underpin the catalytic interface between active site and multimetallic support. Select examples that provide these fundamental insights include clusters with inorganic $[Fe_4(\mu_4\text{-}O)]$,[17] $[RuCo_3(\mu_3\text{-}O)_4]$,[18] and $[Fe_4(\mu_3\text{-}S)_4]$[19] cores, wherein metal-bound oxo and imido substituents are stabilized by coordinative and electronic participation of a polymetallic support, and a series of

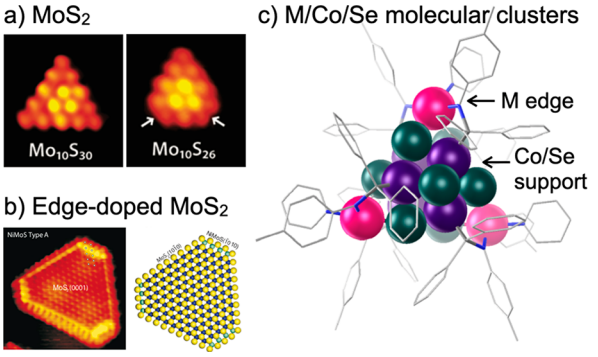

Figure 1. Structural resemblance between (a) MoS_2, (b) edge-doped MoS_2, and (c) M/Co/Se nanoclusters. Panel (a) reproduced with permission from Besenbacher et al. *ACS Nano* **2010**, *4*, 4677−4682. Copyright (2010) American Chemical Society. Panel (b) reproduced with permission from Besenbacher et al. *J. Catal.* **2007**, *249*, 220−233. Copyright (2007) Elsevier.

trinuclear $[Fe_3]$ and $[Cr_3]$ clusters in which electronic coupling between the metal centers facilitates cooperative, multisite reactivity.[20,21] Catalytically active chalcogenide clusters are scarce, including $[Mo_3S_{13}]^{2-}$ and $[MoFe_3(\mu_3\text{-}S)_4]$, for hydrogen evolution and hydrazine reduction,[22,23] respectively, whereas metallic or metal oxide molecular clusters have been shown to catalyze a wider range of reactions.[24−28] However, the elucidation of catalytic intermediates remains challenging across these platforms and relies heavily on computational modeling as opposed to direct experimental observation.[29,30]

Received: January 8, 2022
Published: May 20, 2022

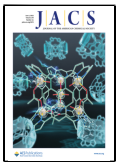

https://doi.org/10.1021/jacs.2c00234
J. Am. Chem. Soc. 2022, 144, 9206−9211

Combining molecular precision and scalability with catalytic competence, we introduced a family of molecular clusters $M_3Co_6Se_8L_6$ (M = Fe, Co, Zn, Sn; L = Ph_2PNTol^-) that incorporate three chemically addressable edge sites (M) on the surface of a Co/Se cluster core.[31−35] This synthetic construct is reminiscent of a broad class of catalytically active edge-doped transition metal dichalcogenide nanomaterials (Figure 1).[6,7,11] Hemilabile edge−support interactions stabilize the three edge sites in protected low-coordinate states,[31] positioning them to function as catalytically active sites and enabling the systematic study of electronic metal−support interactions,[36] as well as allosteric effects[35] and multisite dynamics on the cluster surface. Previously, we discovered that $Fe_3Co_6Se_8L_6$ (**2**) is an excellent catalyst for activating an organic azide and forming CN bonds[37,38] upon transferring the nitrene to *tert*-butyl isocyanide. However, the role of the Fe edges as the catalytically active sites has not been demonstrated.[31] We hypothesized that an earlier transition metal might stabilize the high valent metal-imido intermediates formed in this transformation by localizing oxidation to the edge metals and circumventing the electronic involvement of the Co_6Se_8 support.[31] Leveraging the synthetic versatility of the M/Co/Se construct, a trichromium variant $Cr_3(py)_3Co_6Se_8L_6$ (**1**$(py)_3$, 94% isolated yield; Figure 2) was prepared from the

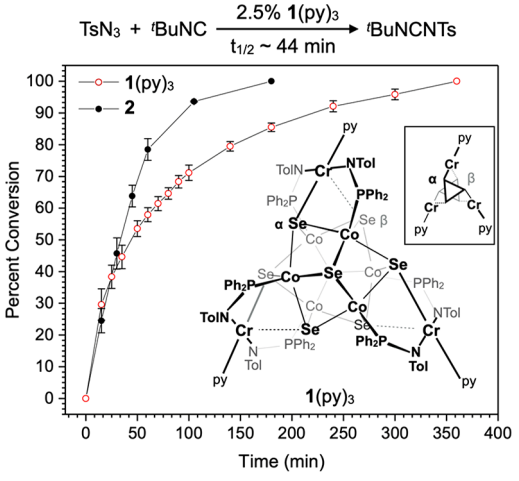

Figure 2. Catalytic carbodiimide formation using nanoclusters **1**$(py)_3$ and **2**, including kinetic monitoring by ^{1}H NMR spectroscopy.

hexalithiated salt $Li_6(py)_6Co_6Se_8L_6$ and $CrCl_2$.[39] Single crystal X-ray diffraction reveals that the 14 e$^-$ square pyramidal Cr(py) edges (Figure 3a) expose open coordination sites for binding substrates at the cluster surface. Like the iron congener, **1**$(py)_3$ is an excellent catalyst for carbodiimide formation (Figure 2).[40] The conversion of tosyl azide (100 equiv) and *tert*-butyl isocyanide (165 equiv) to carbodiimide TsNCN^{t}Bu is completed at room temperature within 6 h of adding the **1**$(py)_3$ (2.5 mol %, 2.8 mM; TOF at $t_{1/2}$ = 27 h^{-1}), slightly slower than in the case of **2** (TOF at $t_{1/2}$ = 34 h^{-1}).

Each Cr edge of the **1**$(py)_3$ cluster rapidly activates tosyl azide, forming three stable Cr-imido units at the cluster surface. In the absence of isocyanide, **1**$(NTs)_3$ (77% isolated yield) is obtained within 15 min of mixing **1**$(py)_3$ with TsN_3 (3 equiv; Scheme 1a). In the solid-state, the Cr(IV) edges adopt a distorted trigonal bipyramidal geometry, with the imido group oriented equatorially (Figure 3b).[41] Each tosyl-imido binds to Cr by N/O-chelation,[42] and as a result the

Scheme 1. Stoichiometric Syntheses of Catalytically Competent Intermediates

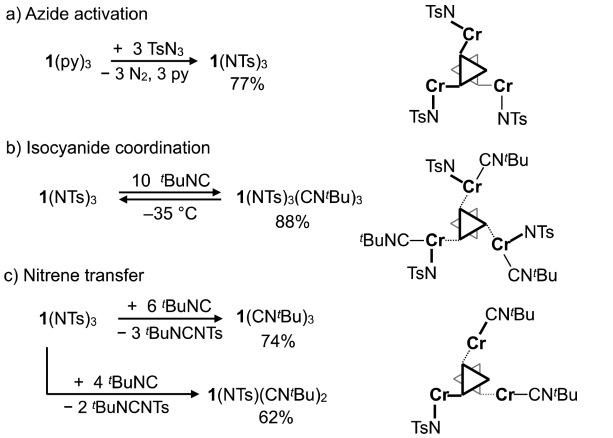

∠Cr−N_{Ts}−S angles are significantly bent (avg. 96°), and the Cr−N_{Ts} double bonds are elongated (avg. 1.82 Å).[43] There is only one other structurally characterized Cr(NTs) complex in the literature,[44] others eluding isolation due to rapid C−H or C−C bond activation.[45,46]

Although the three Cr(NTs) edges have identical first coordination spheres, they are chemically inequivalent due to their (α,α,β) orientation on the Co_6Se_8 surface. Here α and β designate equatorial Se atoms from the top and bottom Co_3Se_4 halves of the cubic Co_6Se_8 support, respectively, as illustrated in the inset of Figure 2.[33] Small variations in the TsN/Cr/Co_6Se_8 bonding interactions structurally distinguish the three edge sites, most notable when comparing the Cr−Se bond lengths of Cr1 with either of Cr2 or Cr3. In solution, the Cr(NTs) edges remain locked in chemically inequivalent orientations even at elevated temperatures, giving rise to multiple N-tosyl ^{1}H NMR environments (Figure S6 and S7). Generally, the low-symmetry (α,α,β) orientation of the edge sites appears to be favored over the previously unobserved (α,α,α) isomer in these nanoclusters.[31,33] We propose this reflects the intrinsic preference of the nanocluster to evenly distribute electron density between the three electron deficient edge centers on the Co_6Se_8 support, and hypothesize this force guides the formation of (α,α,β)-**1**$(NTs)_3$ as the sole isomer upon reaction of **1**$(py)_3$ with azide.

The tris(imido) nanocluster **1**$(NTs)_3$ catalyzes carbodiimide formation similarly to **1**$(py)_3$ (Section S2.2). Stoichiometric studies demonstrate that each of the three edge sites in **1**$(NTs)_3$ can transfer the nitrene group to isocyanide, confirming their viability as catalytically active sites (Scheme 1c). Two equivalents of isocyanide per Cr center (6 equiv total) are required to complete the nitrene transfer from **1**$(NTs)_3$, forming quantitatively the tris(isocyanide) adduct **1**$(CN^tBu)_3$ (74% isolated yield) and carbodiimide TsNCN^{t}Bu (3 equiv). In situ ^{1}H NMR monitoring of this reaction reveals that it unfolds via a stepwise mechanism (Figures 4b and S27). The edge sites engage sequentially to produce carbodiimide, giving rise in the process to two major observable intermediates, which were isolated independently. The first, **1**$(NTs)_3(CN^tBu)_3$, forms upon isocyanide binding at **1**$(NTs)_3$ and was identified as the resting state of the nanocluster under catalytic conditions (Figure S25). This species is consumed over the course of 4 h at room temperature, generating a second, site-differentiated intermediate **1**$(NTs)(CN^tBu)_2$ and

https://doi.org/10.1021/jacs.2c00234
J. Am. Chem. Soc. 2022, 144, 9206−9211

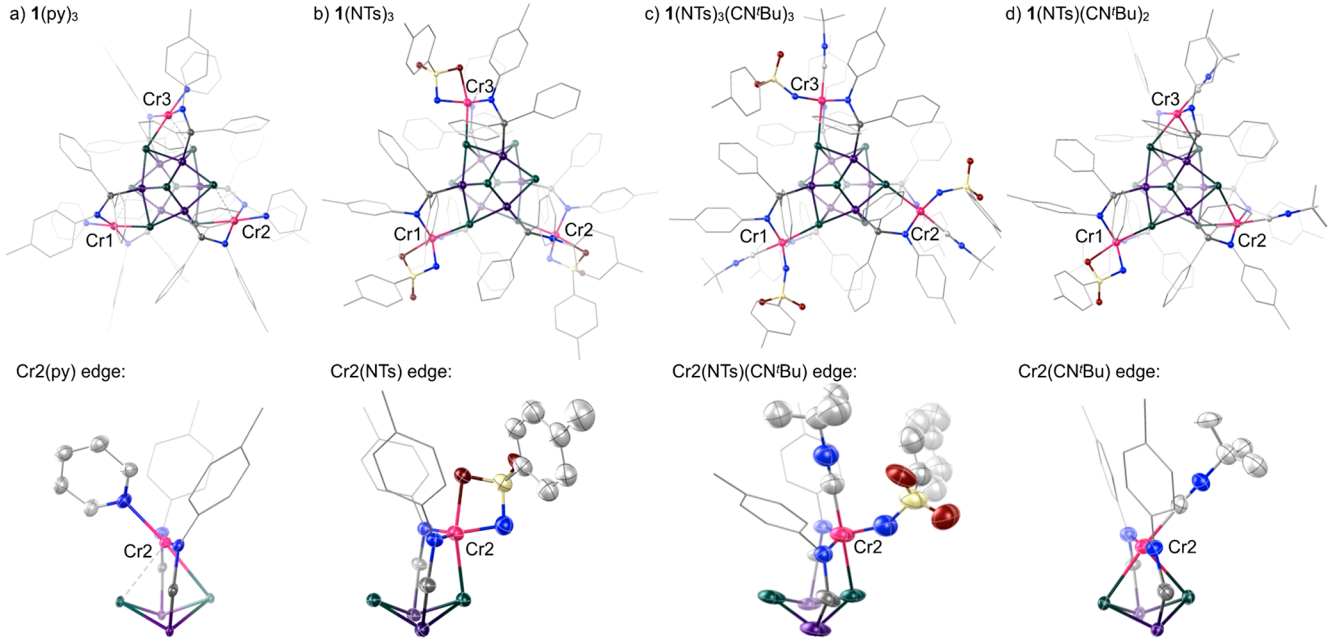

Figure 3. Single crystal X-ray diffraction structures of (a) $\mathbf{1}(py)_3$, (b) $\mathbf{1}(NTs)_3$, (c) $\mathbf{1}(NTs)_3(CN^tBu)_3$, and (d) $\mathbf{1}(NTs)(CN^tBu)_2$. Thermal ellipsoids plotted at 50% probability. H atoms, disordered ligands, and cocrystallized solvents not depicted for clarity.

substoichiometric carbodiimide (2 equiv). Under these conditions, the last equivalent of carbodiimide is released slowly (>48 h at 60 °C) alongside $\mathbf{1}(CN^tBu)_3$.

To independently isolate the first intermediate and unveil the identity of the catalytic resting state, $\mathbf{1}(NTs)_3$ was treated with CN^tBu (10 equiv) at a temperature sufficiently low to prevent the evolution of carbodiimide (−35 °C). Over the course of 24 h, dark red prismatic crystals of the tris(isocyanide)-tris(imido) cluster $\mathbf{1}(NTs)_3(CN^tBu)_3$ formed quantitatively (88% isolated yield, Scheme 1b). Single crystal X-ray diffraction reveals how CN^tBu coordination breaks the N/O-chelation of the N-tosyl group observed in $\mathbf{1}(NTs)_3$ by displacing the sulfonyl oxygen atom to afford a monodentate tosyl imido (Figure 3c). Isocyanide binding at the Cr(NTs) edge strengthens the substrate-edge interactions and weakens the edge-support contacts, trends marked by contracted Cr−NTs bonds (avg. 1.75 vs 1.82 Å) and elongated Cr−Se bonds (avg. 2.61 Å vs 2.48 Å), respectively. We propose that the weakening of edge−support bonding interactions depolarizes the Co_6Se_8 core and provides the necessary structural flexibility for the Cr−Se contacts to reorganize from (α,α,β) in $\mathbf{1}(NTs)_3$ to the (α,α,α) configuration in $\mathbf{1}(NTs)_3(CN^tBu)_3$ in which all edge sites are identical.

Rather than extruding three equivalents of carbodiimide, $\mathbf{1}(NTs)_3(CN^tBu)_3$ evolves to a second intermediate that contains a single $Cr^{IV}(NTs)$ edge free of bound isocyanide (Figure S27). Its identity as $\mathbf{1}(NTs)(CN^tBu)_2$ was elucidated by independent synthesis (62% isolated yield) from $\mathbf{1}(NTs)_3$ and substoichiometric CN^tBu (4 equiv; Scheme 1c), and its catalytic competence demonstrated (Section S2.2). Unlike $\mathbf{1}(NTs)_3(CN^tBu)_3$, the mono(imido) $\mathbf{1}(NTs)(CN^tBu)_2$ is indefinitely stable at room temperature, evidence of the high affinity for isocyanide of the two Cr(II) sites which do not release isocyanide that would otherwise strip the nitrene off the Cr(NTs) edge. Despite this high affinity, the Cr−CN^tBu bonding interactions in $\mathbf{1}(NTs)(CN^tBu)_2$ are among the longest reported (avg. 2.08 Å),[47] and the CN stretching frequency (ν_{CN} = 2196 cm^{-1}) is blue-shifted, a mark of the electron deficiency of these Cr centers which do not engage in π-backbonding.

Comparing the Cr(NTs) site in $\mathbf{1}(NTs)(CN^tBu)_2$ with those of $\mathbf{1}(NTs)_3$ we discovered that the chemical state of the neighboring active sites on the cluster impact its structure and reactivity. Although of identical coordination environment to those in $\mathbf{1}(NTs)_3$, the Cr(NTs) edge in $\mathbf{1}(NTs)(CN^tBu)_2$ features a strengthened Cr−Se interaction (2.444(2) vs 2.48 avg. Å) and an elongated Cr−N_{Ts} bond (1.862(9) vs 1.82 avg. Å; Figure 3d) in the solid state. To probe if the strengthened edge−support interaction decreases nitrene transfer reactivity of the Cr(NTs) edge, the isocyanide binding affinities of $\mathbf{1}(NTs)_3$ and $\mathbf{1}(NTs)(CN^tBu)_2$ were compared. Using ^1H NMR spectroscopy, the binding constant for isocyanide at the $\mathbf{1}(NTs)_3$ cluster to produce $\mathbf{1}(NTs)_3(CN^tBu)_{1-3}$ adducts is estimated to average 44(7) M^{-1} for the three sites, whereas there is no spectroscopic evidence of any isocyanide binding at the Cr(NTs) site in $\mathbf{1}(NTs)(CN^tBu)_2$ under identical conditions (see SI, Section S4). We propose that structural differentiation with $Cr^{II}(CN^tBu)$ edge sites slows nitrene transfer kinetics at this third edge site, distinguishing its reactivity from that of the first Cr(NTs) edge. The strengthened edge−support interactions in $\mathbf{1}(NTs)(CN^tBu)_2$ are also associated with a reorganization back to (α,α,β) symmetry in the solid state. This rearrangement reinforces the hypothesis that α/β isomerism enables the Co_6Se_8 support to reversibly distribute electron density via structural changes in response to substrate binding events at the active sites.

Informed by the catalytic and stoichiometric reactivity of the trichromium nanoclusters, a catalytic cycle is proposed at a single edge site (Figure 4a). The cycle begins with a $Cr^{II}L'$ (L′ = py, CN^tBu) site that quickly activates tosyl azide, producing a $Cr^{IV}(NTs)$ species. Isocyanide binding to $Cr^{IV}(NTs)$ disrupts the N/O-chelation of the N-tosyl group, and generates the catalytic resting state $Cr^{IV}(NTs)(CN^tBu)$. Although both coupling substrates are already bound at the $Cr^{IV}(NTs)$-

https://doi.org/10.1021/jacs.2c00234
J. Am. Chem. Soc. 2022, 144, 9206−9211

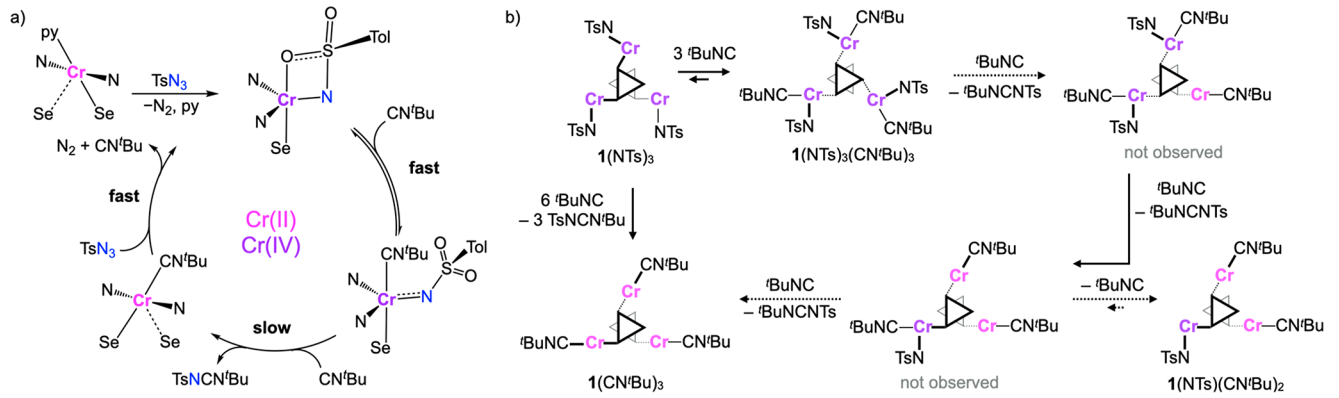

Figure 4. (a) Proposed catalytic cycle for carbodiimide formation at an isolated Cr edge site. (b) Differentiated nitrene transfer reactivity at the three edge sites of $\mathbf{1}(NTs)_3$ under stoichiometric conditions.

(CN^tBu) edge, an additional equivalent of isocyanide is required for carbodiimide formation to occur. Extrusion of carbodiimide is the rate determining step and regenerates the $Cr^{II}(CN^tBu)$ site, which is ready to reengage with azide.

Electronic and structural differences distinguish the individual Cr edge sites of the nanocluster, leading to interdependent and sequential reactivity that is observable under stoichiometric conditions. The stepwise process of transferring the nitrene groups from $\mathbf{1}(NTs)_3$ is detailed in Figure 4b, informed by the observation and isolation of $\mathbf{1}(NTs)_3(CN^tBu)_3$ and $\mathbf{1}(NTs)(CN^tBu)_2$. We propose that as the $Cr^{II}(CN^tBu)$ edges are generated on the nanocluster, they have a stabilizing effect on the neighboring $Cr^{IV}(NTs)$ sites, deactivating them toward isocyanide binding and, consequently, nitrene transfer. Throughout the catalytic cycle, the inorganic Co/Se support is structurally responsive to substrate activation and transfer with hemilabile Cr−Se interactions enabling facile transitions between κ^3 and κ^4 binding to accommodate the Cr edge sites in diverse configurations.

The dichotomy between the stability of the Cr(NTs) edges in the Cr/Co/Se clusters toward isolation and their propensity to accomplish group transfer catalytically is unusual and uniquely positions this system for mechanistic investigations. Only two other imido-bound transition metal-chalcogenide clusters have been previously reported, the cubane-type $Fe_4S_4(NR)$ and $Mo_4S_4(NR)_4$ clusters,[19,48] though neither have been shown to be catalytically competent or active toward stoichiometric group transfer chemistry. **1** is not only a functional model for heterogeneous single-atom group transfer catalysis, but also a powerful platform to study the dynamics of neighboring active sites in heterogeneous catalysts. While the push−pull dynamic between the substrate/edge/support is central to completing a catalytic cycle at an isolated Cr edge site, a domino effect wherein electronic changes propagate through the Co_6Se_8 support intertwines the reactivity of neighboring active sites. Overall, this study sheds light on the mechanism of nitrene transfer at the surface of a well-defined nanocluster catalyst bearing three operational active sites, achieving a distinguished level of detail for nanocluster catalysis.

■ ASSOCIATED CONTENT

Supporting Information

The Supporting Information is available free of charge at https://pubs.acs.org/doi/10.1021/jacs.2c00234.

^{1}H NMR and IR spectra for all compounds, crystallographic data, catalytic and stoichiometric nitrene transfer experiments, as well as binding constant analysis (PDF)

Accession Codes

CCDC 2131446−2131448 and 2172819 contain the supplementary crystallographic data for this paper. These data can be obtained free of charge via www.ccdc.cam.ac.uk/data_request/cif, or by emailing data_request@ccdc.cam.ac.uk, or by contacting The Cambridge Crystallographic Data Centre, 12 Union Road, Cambridge CB2 1EZ, UK; fax: +44 1223 336033.

■ AUTHOR INFORMATION

Corresponding Author

Alexandra Velian − *Department of Chemistry, University of Washington, Seattle, Washington 98195, United States;* orcid.org/0000-0002-6782-7139; Email: avelian@uw.edu

Authors

Jonathan A. Kephart − *Department of Chemistry, University of Washington, Seattle, Washington 98195, United States;* orcid.org/0000-0003-4608-1160

Benjamin S. Mitchell − *Department of Chemistry, University of Washington, Seattle, Washington 98195, United States;* orcid.org/0000-0001-6585-2237

Werner Kaminsky − *Department of Chemistry, University of Washington, Seattle, Washington 98195, United States;* orcid.org/0000-0002-9100-4909

Complete contact information is available at: https://pubs.acs.org/10.1021/jacs.2c00234

Notes

The authors declare no competing financial interest.

■ ACKNOWLEDGMENTS

The authors thank P. Gannon and D. Rogers (UW Chemistry) for assistance with X-ray diffraction measurements. This work was supported by the National Science Foundation (NSF) through a Faculty Early Career Development Program Award (1944843) and by the Research Corporation for Science Advancement through a Cottrell Scholars Award. The X-ray crystallography facility was funded through NSF Grant 0840520. B.S.M. is grateful for support from the NSF Graduate Research Fellowship Program.

REFERENCES

(1) Nørskov, J. K.; Bligaard, T.; Hvolbæk, B.; Abild-Pedersen, F.; Chorkendorff, I.; Christensen, C. H. The Nature of the Active Site in Heterogeneous Metal Catalysis. *Chem. Soc. Rev.* **2008**, *37* (10), 2163−2171.

(2) Tyo, E. C.; Vajda, S. Catalysis by Clusters with Precise Numbers of Atoms. *Nat. Nanotechnol.* **2015**, *10* (7), 577−588.

(3) Du, X.; Jin, R. Atomically Precise Metal Nanoclusters for Catalysis. *ACS Nano* **2019**, *13* (7), 7383−7387.

(4) Taylor, H. S.; Armstrong, E. F. A Theory of the Catalytic Surface. *Proc. R. Soc. London Ser. Contain. Pap. Math. Phys. Character* **1925**, *108* (745), 105−111.

(5) Zambelli, T.; Wintterlin, J.; Trost, J.; Ertl, G. Identification of the "Active Sites" of a Surface-Catalyzed Reaction. *Science* **1996**, *273* (5282), 1688−1690.

(6) Tuxen, A.; Kibsgaard, J.; Gøbel, H.; Lægsgaard, E.; Topsøe, H.; Lauritsen, J. V.; Besenbacher, F. Size Threshold in the Dibenzothiophene Adsorption on MoS_2 Nanoclusters. *ACS Nano* **2010**, *4* (8), 4677−4682.

(7) Lauritsen, J.; Kibsgaard, J.; Olesen, G.; Moses, P.; Hinnemann, B.; Helveg, S.; Norskov, J.; Clausen, B.; Topsoe, H.; Lagsgaard, E.; Besenbacher, F. Location and Coordination of Promoter Atoms in Co- and Ni-Promoted MoS_2-Based Hydrotreating Catalysts. *J. Catal.* **2007**, *249* (2), 220−233.

(8) Jaramillo, T. F.; Jorgensen, K. P.; Bonde, J.; Nielsen, J. H.; Horch, S.; Chorkendorff, I. Identification of Active Edge Sites for Electrochemical H_2 Evolution from MoS_2 Nanocatalysts. *Science* **2007**, *317* (5834), 100−102.

(9) Xu, Z.; Xiao, F.-S.; Purnell, S. K.; Alexeev, O.; Kawi, S.; Deutsch, S. E.; Gates, B. C. Size-Dependent Catalytic Activity of Supported Metal Clusters. *Nature* **1994**, *372* (6504), 346−348.

(10) Zhao, S.; Austin, N.; Li, M.; Song, Y.; House, S. D.; Bernhard, S.; Yang, J. C.; Mpourmpakis, G.; Jin, R. Influence of Atomic-Level Morphology on Catalysis: The Case of Sphere and Rod-Like Gold Nanoclusters for CO_2 Electroreduction. *ACS Catal.* **2018**, *8* (6), 4996−5001.

(11) Kibsgaard, J.; Tuxen, A.; Knudsen, K. G.; Brorson, M.; Topsøe, H.; Lægsgaard, E.; Lauritsen, J. V.; Besenbacher, F. Comparative Atomic-Scale Analysis of Promotional Effects by Late 3d-Transition Metals in MoS_2 Hydrotreating Catalysts. *J. Catal.* **2010**, *272* (2), 195−203.

(12) Hong, X.; Chan, K.; Tsai, C.; Nørskov, J. K. How Doped MoS_2 Breaks Transition-Metal Scaling Relations for CO_2 Electrochemical Reduction. *ACS Catal.* **2016**, *6* (7), 4428−4437.

(13) Abbasi, P.; Asadi, M.; Liu, C.; Sharifi-Asl, S.; Sayahpour, B.; Behranginia, A.; Zapol, P.; Shahbazian-Yassar, R.; Curtiss, L. A.; Salehi-Khojin, A. Tailoring the Edge Structure of Molybdenum Disulfide toward Electrocatalytic Reduction of Carbon Dioxide. *ACS Nano* **2017**, *11* (1), 453−460.

(14) Degroot, M. W.; Corrigan, J. F. High Nuclearity Clusters: Metal-Chalcogenide Polynuclear Complexes. In *Comprehensive Coordination Chemistry II*; Elsevier, 2003; pp 57−123. DOI: 10.1016/B0-08-043748-6/06147-8.

(15) Anyushin, A. V.; Kondinski, A.; Parac-Vogt, T. N. Hybrid Polyoxometalates as Post-Functionalization Platforms: From Fundamentals to Emerging Applications. *Chem. Soc. Rev.* **2020**, *49* (2), 382−432.

(16) Jin, R.; Zeng, C.; Zhou, M.; Chen, Y. Atomically Precise Colloidal Metal Nanoclusters and Nanoparticles: Fundamentals and Opportunities. *Chem. Rev.* **2016**, *116* (18), 10346−10413.

(17) Reed, C. J.; Agapie, T. A Terminal Fe^{III}-Oxo in a Tetranuclear Cluster: Effects of Distal Metal Centers on Structure and Reactivity. *J. Am. Chem. Soc.* **2019**, *141* (24), 9479−9484.

(18) Amtawong, J.; Balcells, D.; Wilcoxen, J.; Handford, R. C.; Biggins, N.; Nguyen, A. I.; Britt, R. D.; Tilley, T. D. Isolation and Study of Ruthenium-Cobalt Oxo Cubanes Bearing a High-Valent, Terminal Ru^{V}-Oxo with Significant Oxyl Radical Character. *J. Am. Chem. Soc.* **2019**, *141* (50), 19859−19869.

(19) Sridharan, A.; Brown, A. C.; Suess, D. L. M. A Terminal Imido Complex of an Iron-Sulfur Cluster. *Angew. Chem., Int. Ed.* **2021**, *60* (23), 12802−12806.

(20) Bartholomew, A. K.; Juda, C. E.; Nessralla, J. N.; Lin, B.; Wang, S. G.; Chen, Y.; Betley, T. A. Ligand-Based Control of Single-Site vs. Multi-Site Reactivity by a Trichromium Cluster. *Angew. Chem., Int. Ed.* **2019**, *58* (17), 5687−5691.

(21) Powers, T. M.; Betley, T. A. Testing the Polynuclear Hypothesis: Multielectron Reduction of Small Molecules by Triiron Reaction Sites. *J. Am. Chem. Soc.* **2013**, *135* (33), 12289−12296.

(22) Kibsgaard, J.; Jaramillo, T. F.; Besenbacher, F. Building an Appropriate Active-Site Motif into a Hydrogen-Evolution Catalyst with Thiomolybdate $[Mo_3S_{13}]^{2-}$ Clusters. *Nat. Chem.* **2014**, *6* (3), 248−253.

(23) Coucouvanis, D.; Mosier, P. E.; Demadis, K. D.; Patton, S.; Malinak, S. M.; Kim, C. G.; Tyson, M. A. The Catalytic Reduction of Hydrazine to Ammonia by the $MoFe_3S_4$ Cubanes and Implications Regarding the Function of Nitrogenase. Evidence for Direct Involvement of the Molybdenum Atom in Substrate Reduction. *J. Am. Chem. Soc.* **1993**, *115* (25), 12193−12194.

(24) Luo, Z.; Castleman, A. W.; Khanna, S. N. Reactivity of Metal Clusters. *Chem. Rev.* **2016**, *116* (23), 14456−14492.

(25) Carr, C. R.; Taheri, A.; Berben, L. A. Fast Proton Transfer and Hydrogen Evolution Reactivity Mediated by $[Co_{13}C_2(CO)_{24}]^{4-}$. *J. Am. Chem. Soc.* **2020**, *142* (28), 12299−12305.

(26) Jin, R.; Li, G.; Sharma, S.; Li, Y.; Du, X. Toward Active-Site Tailoring in Heterogeneous Catalysis by Atomically Precise Metal Nanoclusters with Crystallographic Structures. *Chem. Rev.* **2021**, *121* (2), 567−648.

(27) Chen, Y.; Wu, C.; Sung, P.; Chan, S. I.; Chen, P. P. Turnover of a Methane Oxidation Tricopper Cluster Catalyst: Implications for the Mechanism of the Particulate Methane Monooxygenase (PMMO). *ChemCatChem.* **2020**, *12* (11), 3088−3096.

(28) Song, F.; Moré, R.; Schilling, M.; Smolentsev, G.; Azzaroli, N.; Fox, T.; Luber, S.; Patzke, G. R. $\{Co_4O_4\}$ and $\{Co_xNi_{4-x}O_4\}$ Cubane Water Oxidation Catalysts as Surface Cut-Outs of Cobalt Oxides. *J. Am. Chem. Soc.* **2017**, *139* (40), 14198−14208.

(29) Luo, Z.; Khanna, S. N. Metal Cluster Catalysis. In *Metal Clusters and Their Reactivity*; Springer Singapore: Singapore, 2020; pp 215−239. DOI: 10.1007/978-981-15-9704-6_13.

(30) Ren, Y.; Yang, Y.; Zhao, Y.-X.; He, S.-G. Conversion of Methane with Oxygen to Produce Hydrogen Catalyzed by Triatomic Rh_3^- Cluster Anion. *JACS Au* **2022**, *2* (1), 197−203.

(31) Kephart, J. A.; Mitchell, B. S.; Chirila, A.; Anderton, K. J.; Rogers, D.; Kaminsky, W.; Velian, A. Atomically Defined Nano-Propeller $Fe_3Co_6Se_8(Ph_2PNTol)_6$: Functional Model for the Electronic Metal-Support Interaction Effect, and High Catalytic Activity for Carbodiimide Formation. *J. Am. Chem. Soc.* **2019**, *141* (50), 19605−19610.

(32) Kephart, J. A.; Boggiano, A. C.; Kaminsky, W.; Velian, A. Inorganic Clusters as Metalloligands: Ligand Effects on the Synthesis and Properties of Ternary Nanopropeller Clusters. *Dalton Trans.* **2020**, *49* (45), 16464−16473.

(33) Kephart, J. A.; Romero, C. G.; Tseng, C.-C.; Anderton, K. J.; Yankowitz, M.; Kaminsky, W.; Velian, A. Hierarchical Nanosheets Built from Superatomic Clusters: Properties, Exfoliation and Single-Crystal-to-Single-Crystal Intercalation. *Chem. Sci.* **2020**, *11* (39), 10744−10751.

(34) Mitchell, B. S.; Kaminsky, W.; Velian, A. Tuning the Electronic Structure of Atomically Precise Sn/Co/Se Nanoclusters via Redox Matching of Tin(IV) Surface Sites. *Inorg. Chem.* **2021**, *60* (9), 6135−6139.

(35) Mitchell, B. S.; Krajewski, S. M.; Kephart, J. A.; Rogers, D.; Kaminsky, W.; Velian, A. Redox-Switchable Allosteric Effects in Molecular Clusters. *JACS Au* **2022**, *2* (1), 92−96.

(36) Campbell, C. T. Catalyst-Support Interactions: Electronic Perturbations. *Nat. Chem.* **2012**, *4* (8), 597−598.

https://doi.org/10.1021/jacs.2c00234
J. Am. Chem. Soc. 2022, 144, 9206−9211

(37) Hili, R.; Yudin, A. K. Making Carbon-Nitrogen Bonds in Biological and Chemical Synthesis. *Nat. Chem. Biol.* **2006**, *2* (6), 284−287.
(38) Kennemur, J. G.; Novak, B. M. Advances in Polycarbodiimide Chemistry. *Polymer* **2011**, *52* (8), 1693−1710.
(39) Kephart, J. A.; Mitchell, B. S.; Kaminsky, W.; Velian, A. Multi-active Site Dynamics on a Molecular Cr/Co/Se Cluster Catalyst. *ChemRxiv*, January 5, 2022. DOI: 10.26434/chemrxiv-2022-zkfsp (accessed on May 16, 2022).
(40) Yousif, M.; Tjapkes, D. J.; Lord, R. L.; Groysman, S. Catalytic Formation of Asymmetric Carbodiimides at Mononuclear Chromium(II/IV) Bis(Alkoxide) Complexes. *Organometallics* **2015**, *34* (20), 5119−5128.
(41) Dong, Y.; Clarke, R. M.; Zheng, S.-L.; Betley, T. A. Synthesis and Electronic Structure Studies of a Cr-Imido Redox Series. *Chem. Commun.* **2020**, *56* (21), 3163−3166.
(42) Laskowski, C. A.; Hillhouse, G. L. Group-Transfer Reactions of Ni(II)-Ni(II) Bridging Imido Complexes. Catalytic Formation of Carbodiimides and Isocyanates via Nitrene Transfer from Organoazides. *Organometallics* **2009**, *28* (20), 6114−6120.
(43) A search for all Cr···N double bond lengths in the Cambridge Structural Database (updated November 2020) yielded 153 hits between 1.55 and 1.874 Å (mean 1.65(3) Å). A similar search for Cr···N single bond lengths yielded 3786 hits between 1.763 and 2.443 Å (mean 2.06(9) Å).
(44) Zdilla, M. J.; Abu-Omar, M. M. Mechanism of Catalytic Aziridination with Manganese Corrole: The Often Postulated High-Valent Mn(V) Imido Is Not the Group Transfer Reagent. *J. Am. Chem. Soc.* **2006**, *128* (51), 16971−16979.
(45) Zhou, W.; Patrick, B. O.; Smith, K. M. Influence of Redox Non-Innocent Phenylenediamido Ligands on Chromium Imido Hydrogen-Atom Abstraction Reactivity. *Chem. Commun.* **2014**, *50* (69), 9958−9960.
(46) Heins, S. P.; Morris, W. D.; Wolczanski, P. T.; Lobkovsky, E. B.; Cundari, T. R. Nitrene Insertion into C-C and C-H Bonds of Diamide Diimine Ligands Ligated to Chromium and Iron. *Angew. Chem., Int. Ed.* **2015**, *54* (48), 14407−14411.
(47) A search for all Cr···C(CN^tBu) bond lengths in the Cambridge Structural Database (updated November 2020) yielded 53 hits between 1.87 and 2.068 Å (mean 1.97(3) Å).
(48) Hogarth, G.; Richards, I. Regioselective and Reversible Carbon-Nitrogen Bond Formation: Synthesis, Structure and Reactivity of Ureato-Bridged Complexes $[Mo_2(NAr)_2(\mu\text{-}X)\{\mu\text{-}ArNC(O)NAr\}(S_2CNR_2)_2]$ (Ar = Ph, p-Tol; X = S, NAr; R = Me, Et, Pr). *Dalton Trans.* **2005**, *4*, 760−773.

https://doi.org/10.1021/jacs.2c00234
J. Am. Chem. Soc. 2022, 144, 9206−9211